A secondary clump of red giant stars: why and where

Léo Girardi

Max-Planck-Institut für Astrophysik, Karl-Schwarzschild-Str. 1, D-85740 Garching bei München, Germany
E-mail: leo@mpa-garching.mpg.de

submitted to Monthly Notices of the Royal Astronomical Society

Abstract. Based on the results of detailed population synthesis models, Girardi et al. (1998) recently claimed that the clump of red giants in the colour–magnitude diagram (CMD) of composite stellar populations should present an extension to lower luminosities, which goes down to about 0.4 mag below the main clump. This feature is made of stars just massive enough for having ignited helium in non-degenerate conditions, and therefore corresponds to a limited interval of stellar masses and ages. In the present models, which include moderate convective overshooting, it corresponds to ~ 1 Gyr old populations.
In this paper, we go into more details about the origin and properties of this feature. We first compare the clump theoretical models with data for clusters of different ages and metallicities, basically confirming the predicted behaviours. We then refine the previous models in order to show that: (i) The faint extension is expected to be clearly separated from the main clump in the CMD of metal-rich populations, defining a 'secondary clump' by itself. (ii) It should be present in all galactic fields containing ~ 1 Gyr old stars and with mean metallicities higher than about $Z = 0.004$. (iii) It should be particularly strong, if compared to the main red clump, in galaxies which have increased their star formation rate in the last Gyr or so of their evolution. In fact, secondary clumps similar to the model predictions are observed in the CMD of nearby stars from *Hipparcos* data, and in those of some Large Magellanic Cloud fields observed to date. There are also several reasons why this secondary clump may be missing or hidden in other observed CMDs of galaxy fields. For instance, it becomes undistinguishable from the main clump if the photometric errors or differential absorption are larger than about 0.2 mag. Nonetheless, this structure may provide important constraints to the star formation history of Local Group galaxies. We comment also on the intrinsic luminosity variation and dispersion of clump stars, which may limit their use as either absolute or relative distance indicators, respectively.

Key words: stars: evolution – Hertzsprung-Russell (HR) diagram – stars:horizontal branch – stars: luminosity function, mass function – Magellanic Clouds – galaxies: stellar content

1. Introduction

Since the works by Cannon (1970) and Faulkner & Cannon (1973), the clump of red giants in the colour–magnitude diagram (CMD) of intermediate-age and old open clusters is recognised as being formed by stars in the stage of central helium burning (CHeB). The near constancy of the clump absolute magnitude in these clusters was correctly interpreted as the result of He-ignition in a electron-degenerate core. Under these conditions, He-burning can not start until the stellar core mass attains a critical value of about 0.45 $M_\odot$. It then follows that all low-mass stars (i.e. those which develop a degenerate He-core after H-exhaustion) have similar core masses at the beginning of He-burning, and hence similar luminosities.

The red giant clump is also a remarkable feature in the CMD of composite stellar populations, like the fields of nearby galaxies. Since the clumps of all stellar populations older than about 1 Gyr fall in the same region of the CMD, they define a feature usually as striking to the eye as the main sequence. Recently, the *Hipparcos* data allowed to clearly see the clump in the CMD of nearby stars (Perryman et al. 1997).

Due to its origin and the nearly constancy in luminosity, the red clump has been usually considered to contain few information about its parent population. Its use as a distance indicator has been proposed by Cannon (1970), and since then applied by several authors, like e.g. Seidel, Da Costa & Demarque (1987), Hatzidimitriou & Hawkins (1989) and others. It has been recently re-proposed by Paczyński & Stanek (1998), following the release of the *Hipparcos* catalogue. Indeed, the mean absolute magnitude of the clump defined by *Hipparcos* can be measured with a precision of hundredths of magnitude, and used as a reference for $(m-M)_0$ determinations. The apparent constancy of the I_0 magnitude with the $V-I$ colour inside the clump, in different stellar systems, was considered as evidence that the mean clump absolute magnitude $M_I^{\rm cl}$ does not depend on metallicity (Paczyński & Stanek 1998; Stanek & Garnavich 1998; Udalski et al. 1998; Stanek, Zaritsky & Harris 1998). This conclusion, however, has been questioned by Girardi et al. (1998; hereafter Paper I). They made use of a large set of evolutionary tracks to show that more massive clump stars are systematically bluer than the less massive ones, so that the colour range spanned by the *Hipparcos* clump is largely caused by the dispersion of masses (and hence ages) of local stars, and not simply by their metallicity. In this case, the constancy of the mean clump I-band magnitude with colour can be simply reproduced by models, and understood as the result of age segregation inside the clump. $M_I^{\rm cl}$, instead, might be systematically lower (i.e. brighter) for lower metallicities. The model predictions then can be used to provide a first-order correction to distance determinations derived from clump stars (see also Cole 1998). For the LMC, the corrections are such that $(m-M)_0 = 18.28 \pm 0.14$ mag as estimated in Paper I, or $(m-M)_0 = 18.36 \pm 0.17$ mag cf. Cole (1998).

Another prediction of Paper I is that the stars just massive enough for igniting He under non-degenerate conditions, should define a *secondary clumpy feature*, located about 0.3 mag below the clump of the lower-mass stars, and at its blue extremity. A feature similar to the predicted one was found in the CMD from *Hipparcos*.

In this paper, we go into some important details of the theoretical predictions raised in Paper I. First, we briefly recall the underlying stellar evolution theory (Section 2). Then we compare the theoretical behaviour of clump stars with data from stellar clusters of different ages and metallicities (Section 3). This comparison gives support to the behaviour predicted by models. We present simple models for the clump structure in composite stellar populations (Section 4), which predict the appearance of the secondary clump. The conditions for its presence in CMDs of different galaxy fields are examined. We suggest the association of this theoretically predicted feature with some observational ones, and comment on the impact of these results in the interpretation of data for the Magellanic Clouds and other Local Group galaxies. Section 5 summarises the main conclusions.

2. Brief review of the theory

In stars of mass higher than a given value, $M \geq M_{\rm Hef} \sim 2-2.5\ M_\odot$ (see e.g. Chiosi, Bertelli & Bressan 1992), helium ignition takes place under non-degenerate conditions, when the stellar centre attains a critical value of temperature and density. These are the intermediate- and high mass stars. In this case the core mass at helium ignition is a simple monotonically increasing function of stellar mass. The same behaviour holds for the luminosity of the stars during the subsequent core helium burning (CHeB) phase.

In low-mass stars, i.e. those with $M < M_{\rm Hef}$, an electron-degenerate core forms after the central hydrogen exhaustion. Electron conduction reduces the temperature gradient in the core, and the efficient neutrino cooling at the centre makes the temperature maximum to shift to an off-centre region. In this case, the critical temperatures and densities for helium ignition are attained only later in the evolution, when the core mass has grown to a value of about $M_{\rm c} \simeq 0.45\ M_\odot$. This value is nearly constant for the stars with mass lower than about $M_{\rm Hef} - 0.3\ M_\odot$, depending only little on chemical composition and stellar mass. As a result of their similar core masses $M_{\rm c}$, the CHeB phase occurs at similar luminosities for all low-mass stars. However, the helium burning stars of higher masses are slightly hotter than those of lower masses, due to their different envelope masses $M_{\rm env}$. Higher effective temperatures, and slightly lower luminosities, are also reached at the limit of very low masses, for which $M_{\rm env} \to 0$.

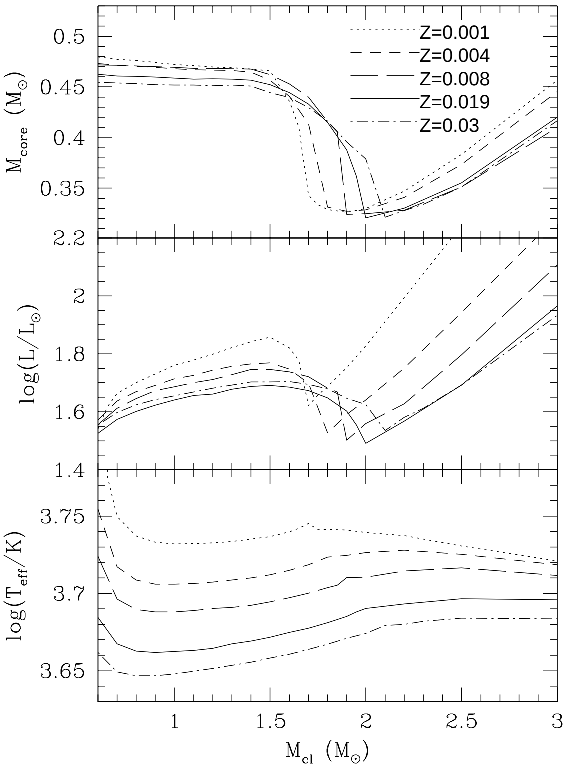

Fig. 1. Stellar parameters at the first stage of quiescent helium burning (i.e. the ZAHB for low-mass stars, or the CHeB stage of lowest luminosity for intermediate-mass ones), as a function of stellar mass and for 5 values of initial metallicity, as derived from Girardi et al. (1999) models. They are: the core mass $M_{\rm c}(M)$ in the upper panel, $\log L(M)$ in the middle, and $\log T_{\rm eff}(M)$ in the lower one.

These behaviours are illustrated in Fig. 1. We plot the values of $M_{\rm c}$, the luminosity L and effective temperature $T_{\rm eff}$ at the initial stage of quiescent CHeB, from the Girardi et al. (1999) stellar models. This point of the stellar tracks coincides with the 'zero-age horizontal branch' (ZAHB) usually defined for low-mass stars, and with the one of minimum luminosity attained during central He-burning for intermediate-mass stars. Some basic characteristics of these stellar tracks have been already described in Girardi & Bertelli (1998) and in Paper I. Suffice it to recall here that they include a moderate amount of convective overshooting from stellar cores.

Table 1. The transition masses $M_{\rm Hef}$ and their corresponding ages $t(M_{\rm Hef})$.

Z	Y	overshoot	$M_{\rm Hef}/M_\odot$	$t(M_{\rm Hef})$/Gyr
0.001	0.230	moderate	1.7	1.22
0.004	0.240	moderate	1.8	1.13
0.008	0.250	moderate	1.9	1.09
0.019	0.273	moderate	2.0	1.13
0.030	0.300	moderate	2.1	1.27
0.019	0.273	no	2.4	0.54

To be noticed in Fig. 1 is that both $M_c(M)$ and $L(M)$ assume a minimum value for $M \sim 2\ M_\odot$, of $M_c \sim 0.33\ M_\odot$ and $\log(L/L_\odot) \simeq 1.5 - 1.6$. The luminosity minimum is used to define the transition masses $M_{\rm Hef}$ referred to in the present work. Their values are indicated in Table 1 for 5 different values of metallicity. The main-sequence lifetime $t(M_{\rm Hef})$ of the corresponding star is also presented. One can notice that whereas $M_{\rm Hef}$ decreases systematically with the metallicity Z, the corresponding transition age $t(M_{\rm Hef})$ is nearly constant (see also Sweigart, Greggio & Renzini 1990 for a detailed discussion of this point), and close to 1.1 Gyr. The $M_{\rm Hef}$ and $t(M_{\rm Hef})$ values we find are typical of models computed with moderate convective overshoot. Additionally, the table presents the same quantities as derived from a set of solar metallicity tracks in which the classical Schwarzschild criterion for convection (i.e. no overshooting) is adopted. In this case, $M_{\rm Hef}$ is about 20 percent larger, whereas $t(M_{\rm Hef})$ about 50 percent lower, than in the case with moderate overshooting.

It is worth recalling that the behaviours presented in Fig. 1 are not exclusive to the Girardi et al. (1999) set of evolutionary tracks. Instead, they are common to models computed either with or without convective overshooting, and regardless of the scheme adopted to deal with the 'breathing pulses of convection' during the late CHeB evolution. The reader is referred to the works by Becker & Iben (1980), Maeder & Meynet (1989), Sweigart et al. (1990), Castellani, Chieffi & Straniero (1992), for similar descriptions of the function $M_c(M)$, which are however based on very different sets of evolutionary tracks. Castellani et al. (1992) also present predictions for $L(M)$ which are similar to the ones described by the present models. Only the stellar models adopting the approximation that M_c is constant for all low-mass ZAHB stars (e.g. Seidel, Demarque & Weinberg 1987) probably do not follow all the trends shown in Fig. 1.

Another important aspect is that the individual stellar tracks, in the mass and metallicity ranges here considered, change little their characteristics during most of the CHeB evolution. This is illustrated in Fig. 2, for the case of solar-metallicity ($Z = 0.019$) CHeB models. In low-mass tracks of $M > 0.8\ M_\odot$, 70 percent of the CHeB lifetime, $t_{\rm He}$, is spent within a box of $\Delta \log L < 0.12$ dex (or $\Delta M_{\rm bol} < 0.3$ mag) by $\Delta \log T_{\rm eff} < 0.006$ dex in the HR diagram. Only at the late stages of CHeB evolution the tracks deviate significantly from their ZAHB positions. A similar situation occurs for intermediate-mass stars, for which an initial phase of fast contraction is followed by a phase of much slower evolution in the HR diagram. As a useful first approximation, we can then consider the locus of these slow-evolution phases in the HR diagram as representative of the behaviour of the complete CHeB tracks of different masses. Finally, we remark that the excursions in temperature during the CHeB phase increase at lower metallicities and masses, but become appreciably higher than the above-mentioned limits only for the tracks with $Z < 0.004$ or with $M < 0.8\ M_\odot$.

From Figs. 1 and 2 (see also figure 1 in Paper I), two clear sequences can be noticed:

- For $M < M_{\rm Hef} = 2\ M_\odot$, and going from higher to lower masses, clump stars have almost constant luminosities at decreasing temperatures. At $M \lesssim 0.9\ M_\odot$, this sequence bends towards much hotter temperatures. The less luminous stars in this mass range are both the most massive (due to their lower core masses) and the less massive ones.
- For $M > M_{\rm Hef}$, and going from lower to higher masses, clump stars have increasing luminosity and almost-constant temperatures. The minimum luminosity, for $M = M_{\rm Hef}$, is about 0.4 mag lower than that of stars with slightly lower mass.

3. The red clump in clusters

The behaviour predicted by the models can be compared to that found in star clusters of different ages and metallicities. The data for clusters in the Magellanic Clouds are particularly useful because their distances and reddening can be considered as constant in a first approximation. Therefore, they allow to infer how the clump luminosity changes as a function of the cluster parameters. Galactic open clusters instead generally suffer from a higher uncertainty in their relative distance modulus.

3.1. The red clump luminosity

Corsi et al. (1994) collected BV data for a dozen LMC clusters, with ages ranging from about 0.2 to 1.2 Gyr, aiming at locating the precise age interval in which the RGB develops in stellar populations. One of the best diagnostics of the development of the RGB is in fact given by the behaviour of the clump luminosity: it increases when the RGB appears and becomes almost constant afterwards. Figure 3 presents the data from Corsi et al. (1994, their table 17) – namely the clump magnitude $V_{\rm cl}$ against that of the termination of the main sequence, $V_{\rm TAMS}$, for each cluster. The vertical lines actually give the possible range of magnitude for the base of the clump, i.e. the one ranging between the mean measured clump, and the faintest clump stars observed in each cluster ($\langle V_{Cl} \rangle$ and $V_{Cl,m}$, respectively, in Corsi et al. 1994 tables). Superimposed, are the relations predicted by Girardi et al. (1999) models for metallicities $Z = 0.004$

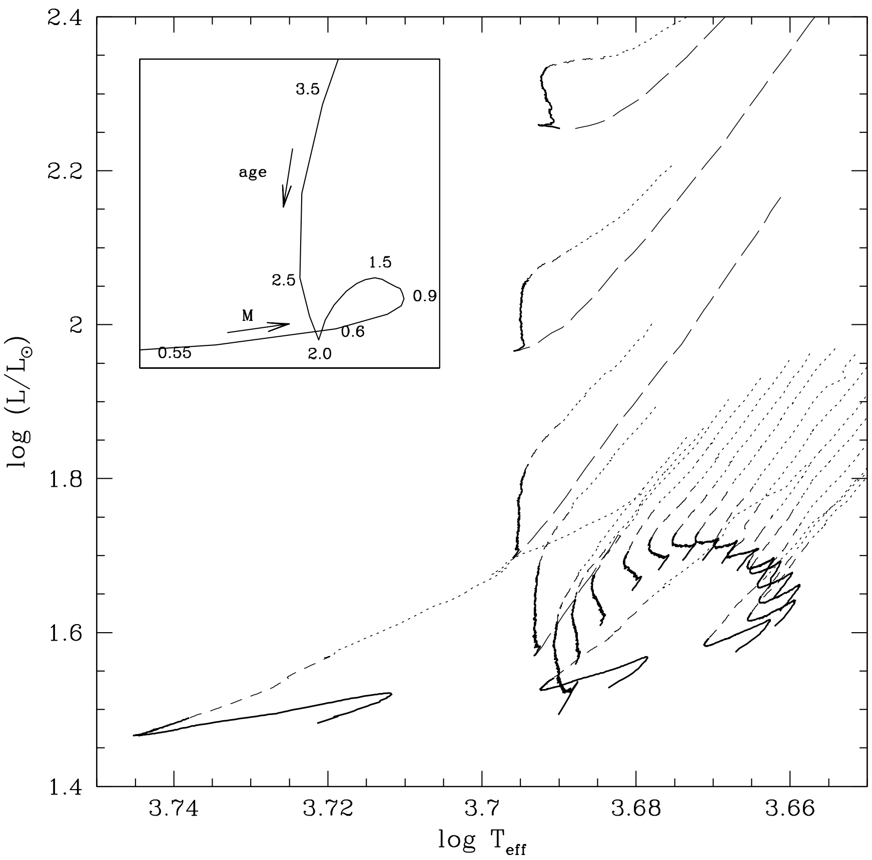

Fig. 2. Evolution of $Z = 0.019$ tracks on the HR diagram during the stage of quiescent CHeB, for several mass values. The solid lines denote the evolution during most of the CHeB lifetime: for low-mass stars, they start when the gravitational contraction provides less than 1 percent of the stellar luminosity (it corresponds to the stage of ZAHB), whereas for intermediate-mass stars they begin at the CHeB stage of lowest luminosity. In both cases, the lines end when 70 percent of the CHeB lifetime $t_{\rm He}$ is reached. Thus, these solid lines correspond to most of the clump red giants (or to the horizontal branch in the limit of lowest masses). Dashed and dotted lines illustrate phases of faster evolution during the CHeB. The short-dashed lines denote the evolution from 70 percent up to 85 percent of $t_{\rm He}$, whereas the dotted ones go up to 99 percent of $t_{\rm He}$. Moreover, the long-dashed lines present the initial stage of quiescent CHeB of intermediate-mass stars; in the mass range here plotted ($M \leq 3.5\ M_{\odot}$), this phase never exceeds 12 percent of $t_{\rm He}$. The insert shows schematically how the stellar masses and ages vary along the sequence of CHeB models. Some representative mass values (in $M_{\odot}$) are indicated along this line.

and 0.008, at the stage of the lowest luminosity during the CHeB (cf. also Fig. 1). The reader should keep in mind that, in the models, the mean clump magnitude is typically located $\lesssim 0.15$ mag above these lines.

The models describe well the behaviour suggested by the data, especially the presence of a minimum in the $V_{\rm cl}(V_{\rm TAMS})$ relation, for $V_{\rm TAMS} \simeq 19.5$, corresponding to the clusters NGC 1868, NGC 2108, NGC 2190 and NGC 2209. Only clusters to the right of this minimum (i.e. older and presumably containing stars with electron-degenerate helium cores), like NGC 2162 and NGC 2173 are found to undoubtedly contain RGB stars (see Corsi et al. 1994; and the comments in Girardi & Bertelli 1998). Of course, different assumptions for the apparent distance modulus of the clusters, or different ways of defining their main sequence termination magnitudes, could change a little the presentation of the data and models in this diagram.

Other recent and homogeneous compilation of clump magnitudes is provided by Udalski (1998b). They collected VI photometry for several intermediate-age and old Magellanic Cloud clusters (with ages from about 1.5 to 12 Gyr), concluding that the clump magnitude $I_0^{\rm cl}$ does not change appreciably in this age range. Together with the results of

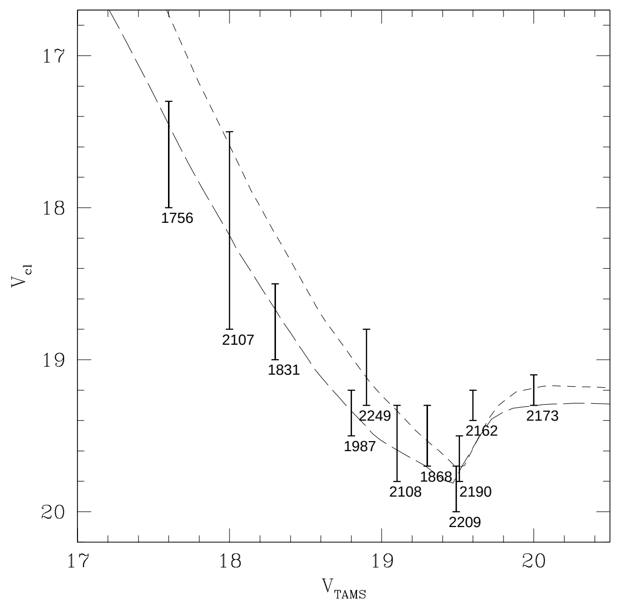

Fig. 3. The behaviour of the clump magnitude $V_{\rm cl}$ as a function of the main sequence termination magnitude $V_{\rm TAMS}$ in LMC clusters, as observed by Corsi et al. (1994), and as predicted by the Girardi et al. (1999) models. The vertical lines link the the mean clump position, with that of its lower extremity (see data in table 17 of Corsi et al. 1994). The NGC numbers of each cluster are indicated. The ages range from about 0.1 to 2 Gyr, from left to right. Sequences of CHeB models (at the stage of initial CHeB, or ZAHB) for $Z=0.008$ and 0.004 are plotted adopting an apparent distance modulus of 18.5 mag. These model lines have the same meaning as indicated in Fig. 1.

Udalski (1998a), these data were used to argue in favour of the mean I-band clump magnitude as a standard candle, and of a low value of the LMC distance modulus – namely 18.18 ± 0.06 mag (see also Udalski et al. 1998; Stanek et al. 1998).

Figure 4 shows Udalski's (1998b, their tables 2, 3 and 4) data for clusters in both Clouds, compared to the results of our models with different metallicities. In plotting the data, we have not applied geometric corrections to the distance modulus of each cluster, as adopted by Udalski. Also, we did not attempt to correct the cluster ages by him presented, in order to put them into a single and consistent age scale. We should keep in mind that age errors as large as 1 Gyr may be present in the data.

The data points present a non-negligible scatter in $I_0^{\rm cl}$, which can not be exclusively attributed to the observational errors. The only clear trend in the data is that the two clusters older than 10 Gyr present clumps fainter by $0.25 - 0.3$ mag with respect to the younger ones.

In Fig. 4 we plot also the model predictions for the mean clump absolute magnitude $M_I^{\rm cl}$ for several metallicities, as determined by properly averaging the luminosity of CHeB stars along the theoretical isochrones. Models were shifted by a constant distance modulus of $(m-M)_0 = 18.3$ mag for the LMC, and 18.7 mag for the SMC, in order to fit the appropriate range of the data..

It is clear that in the age range of $\gtrsim 2$ Gyr, the models predict that the I-band clump magnitude mildly decreases with age, and mildly increases with the metallicity. In order to better compare data and models, we need to consider the age-metallicity relation intrinsic to the cluster data. It is well known that different methods may lead to discrepant metallicity estimates for the same clusters. In the following, we make use only of the metallicity determinations by Olszewski et al. (1991) for the LMC clusters, and Da Costa & Hatzidimitriou (1998) for the SMC ones, whose values are also indicated in Fig. 4. These works made use of the same spectroscopic method for deriving abundance values. Therefore the metallicity scale should be rather homogeneous. For the sake of this homogeneity, we also use the SMC data as expressed in the Zinn & West (1984) scale (see figure 4 in Da Costa & Hatzidimitriou 1998).

For the LMC, the behaviour of the clump magnitude with age indicated by the data seems to be well described by the present models. The only exception is the cluster ESO121 SC03, which apparently presents a too bright clump if compared to our lowest metallicity models. The discrepancy is however not larger than 0.1 mag. Moreover, we should

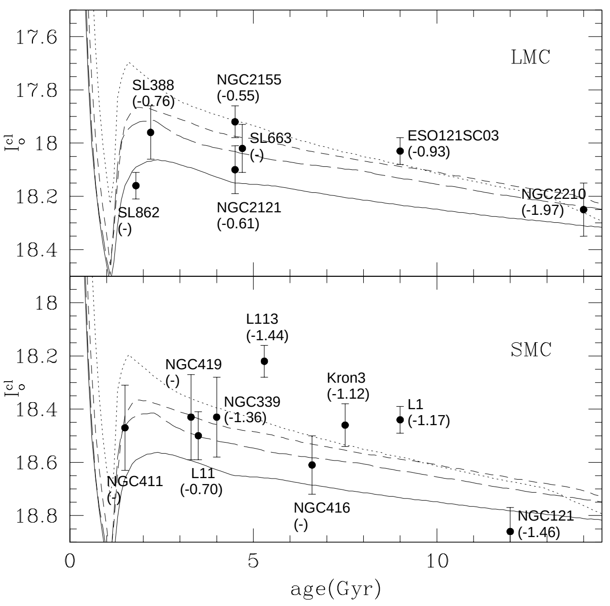

Fig. 4. The behaviour of the clump magnitude as a function of age, in the range from 2 to about 10 Gyr, in both the LMC (upper panel) and the SMC (lower one). The data by Udalski (1998b) are compared to Girardi et al. (1999) models for several metallicities. For each cluster, we indicate the value of [Fe/H] as measured either by Olszewski et al. (1991; for the LMC) or by Da Costa & Hatzidimitriou (1998; for the SMC). The model lines have the same meaning as in Fig. 1: from above to below we have models with metallicities $Z = 0.001$, 0.004, 0.008, and 0.019, corresponding to [Fe/H] $= -1.3$, -0.7, -0.4, and 0, respectively.

keep in mind the unique characteristics of this cluster (see Mateo, Hodge & Schommer 1986): it is located very far from the LMC disk, and is the only known cluster in the LMC with age comprised between 4 Gyr and the classical old clusters with > 12 Gyr (see Da Costa 1991; Olszewski, Suntzeff & Mateo 1996; Geisler et al. 1997). Therefore, it is not clear whether it could really be considered as a member of the LMC disk, and whether it is located at the same distance of the bulk of LMC clusters.

In the SMC, the situation clearly changes. The dispersion of clump magnitudes increases for the clusters in this galaxy, becoming larger than that suggested by the models of different metallicities. What is remarkable is the extremely bright clump of L 113 (~ 0.2 mag brighter than the clusters of similar age), and the faint clump of the cluster NGC 121. In the case of L 113, part of the observed difference could be understood as the result of the apparently anomalous (and low) metallicity of this cluster (see the careful discussion about the SMC age–metallicity relation by Da Costa & Hatzidimitriou 1998), which according to the models would imply a brighter clump. However, the explanation in terms of metallicity differences only would require a much larger dependence of the clump absolute magnitude on metallicity than predicted by the present models. Moreover, a clump so bright is not observed in the case of NGC 339, despite its similar metallicity and age (notice however the large error bar in this latter case). Maybe the key to understanding the clump magnitudes of L 113 and NGC 121, is that these objects are really located at different distances along the line-of-sight. If this is the case for most of the SMC clusters, the comparison with theoretical models under the assumption of a single distance modulus would lose significance.

We conclude that *no firm conclusion about the behaviour of the mean clump absolute magnitude with age and metallicity, for ages larger than 2 Gyr, can be based on the data for so few clusters.* The main problem with LMC data is essentially the lack of bona-fide clusters at the LMC distance with ages between 4 and 12 Gyr. In the case of the SMC, depth effects probably complicate very much the analysis.

On the other hand, we do not find in these data the evidences that model over-estimate the $M_I^{\rm cl}$ dependence on either age or metallicity, as suggested by Udalski (1998ab). In Section 4.7 we further comment on this aspect. We recall that Udalski's conclusions for the SMC clusters were largely based on a data sample for which empirical corrections to the distances were applied. These distance corrections are based on the observed variation of the magnitude of RR Lyrae stars in the neighbouring fields. For clusters like L 1 and L 113, distance corrections of up to ± 0.2 mag were derived by extrapolating the values derived for other lines-of-sight. We regard this procedure, when applied to single clusters, as potential sources of error in the analysis.

3.2. The red clump colour

Another important observational relation is that given by Hatzidimitriou (1991) between the cluster age and the $B-R$ colour difference between the clump and the RGB, d_{B-R}. The good correlation between these quantities allowed her to suggest the use of d_{B-R} as an age indicator for intermediate-age and old star clusters.

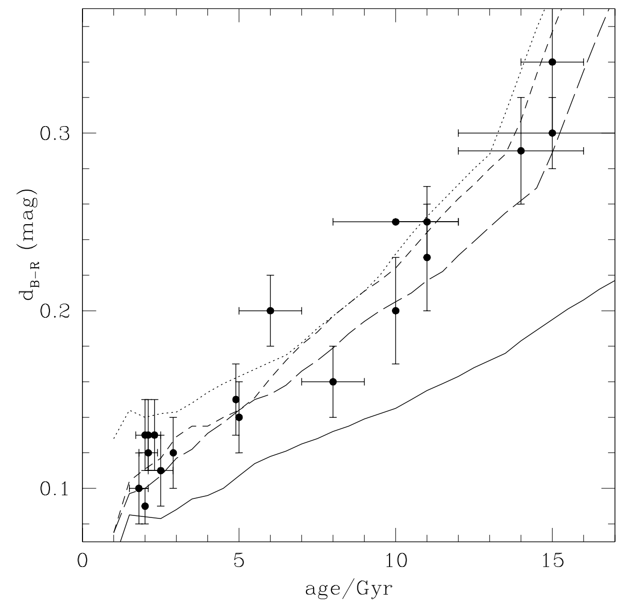

Fig. 5. The behaviour of the colour difference between the mean clump and the RGB at the same level in R, d_{B-R}, as a function of the cluster age, according to the data collected by Hatzidimitriou (1991, her table 1), and the Girardi et al. (1999) models for several metallicities. The lines have the same meaning as indicated in Fig. 1.

Hatzidimitriou's (1991) data sample is shown in Fig. 5. Notice that, in plotting these data, we have made no effort in order to revise the ages of the individual clusters. In fact, the oldest clusters in the sample should better be attributed ages of ~ 12 Gyr, instead of the 15 Gyr shown in the plot, as a result of the recent changes in the absolute age scale of the old globular clusters (see e.g. Gratton et al. 1997; Salaris & Weiss 1997, 1998). In this contest, the age scale presented in Fig. 5 should be considered as a relative one.

The present models for metallicities from $Z = 0.001$ to 0.008 seem to follow a common d_{B-R} vs. age relation, which reproduces well the correlation found in the data. The same does not happen for the $Z = 0.019$ ones, which seem to predict too small d_{B-R} values at a given age. With respect to the data, we remark that only 3 of the clusters plotted in Fig. 5 have metallicities comparable to solar (i.e. with [Fe/H]> -0.3), the remaining ones being more metal poor.

The reason for the $Z = 0.019$ isochrones presenting so low values of d_{B-R}, as compared with the more metal-poor ones, is that for this value of metallicity the bump in the luminosity function along the RGB happens to be located below the luminosity level of the clump. Above this bump, the RGB evolutionary tracks shift to slightly higher temperatures. Therefore, d_{B-R} values get suddenly lower as we go from the $Z = 0.008$ to the $Z = 0.019$ tracks. In the observed CMDs, the reference values of the RGB colour at the level of the clump probably do not take into account this subtle effect, since in these cases the RGB ridge line is drawn by eye, connecting stars both below and above the bump feature. A more detailed comparison with the data would be worth in order to clarify if this effect may be responsible for the apparent discrepancy in the $Z = 0.019$ models. In the present work, we limit ourselves to comment that *the observed trend of d_{B-R} with age is clearly present in the models.* If there is any discrepancy with the observational data, this is in the sense that our most metal-rich models *underestimate* this colour difference.

4. The red clump in galaxies

Once we have tested the model predictions about the clump position in CMDs as a function of age and metallicity, by comparing them with observations of star clusters, we can proceed our modeling of more complex stellar populations.

4.1. Basic theory

The red clump observed in the CMDs of galaxy fields may be described by the sum of those deriving from single-burst stellar populations of different ages and metallicities. In the case of a composite population of single metallicity, if we neglect mass-loss on the RGB, the number $N(M_{\rm cl})\mathrm{d}M_{\rm cl}$ of clump stars with mass in the interval $[M_{\rm cl}, M_{\rm cl}+\mathrm{d}M_{\rm cl}]$, is expressed by

$$N(M_{\rm cl}) \propto \phi_M(M_{\rm cl})\,\psi[T-t(M_{\rm cl})]\,t_{\rm He}(M_{\rm cl}) \quad (1)$$

(see Paper I), where ϕ_M is the IMF, $\psi(T-t)$ is the SFR at the epoch of stellar birth $T-t(M_{\rm cl})$, and $t_{\rm He}$ is the lifetime of the CHeB phase.

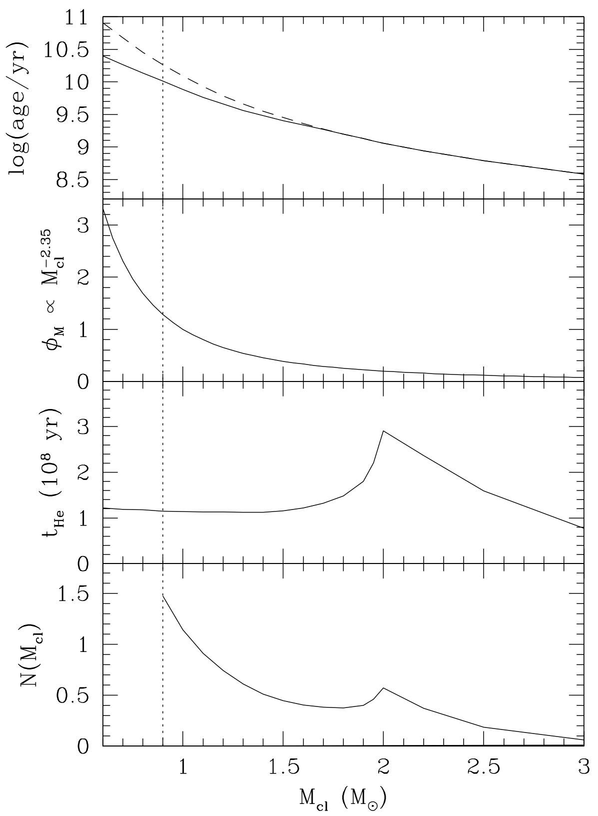

Fig. 6. Quantities which enter into the determination of the mass distribution of clump stars, as derived from $Z=0.008$ tracks. In the panels from top to bottom, we have: (1) the age vs. mass relation, for models assuming mass-loss according to Reimers' (1975) formula with efficiency $\eta=0.4$ (continuous line), and for the alternative case of no mass-loss (dashed line); (2) the Salpeter IMF, $\phi_M \propto M^{-2.35}$, in arbitrary units; (3) the lifetime in the core He-burning phase; and finally (4) the resulting mass distribution, $N(M_{\rm cl})$, in arbitrary units, for the case of a constant SFR during the complete age interval up to 10 Gyr. The vertical dotted line represents the lower mass limit for clump stars in a galaxy field of 10 Gyr and solar metallicity, in the case of Reimers' mass-loss (see upper panel).

Figure 6 shows the quantities which enter into this equation (except for the SFR) as a function of $M_{\rm cl}$, and as derived from our $Z=0.019$ models. To be noticed in the top panel is that the age vs. mass relation for clump stars, $t(M_{\rm cl})$, depends on the amount of mass-loss taken place during the RGB phase. Hence, this function is presented for both the cases (i) of no mass-loss, and (ii) assuming a Reimers' (1975) mass-loss formula with efficiency $\eta = 0.4$ (see Renzini & Fusi Pecci 1988). In the latter case, clump stars of mass lower than 0.90 $M_{\odot}$ would not be present in stellar populations younger than 10 Gyr. This gives an estimate for the lower mass limit of clump stars of solar metallicity. This value would be increased to 1.06 $M_{\odot}$ in the case of no mass-loss. Finally, mass-loss does not affect significantly the stars with $M_{\rm cl} \gtrsim 1.5\ M_{\odot}$.

The second panel from top to bottom presents the Salpeter IMF, with its well-known steep increase for lower-mass stars. We notice that also this function should be slightly corrected in order to consider mass-loss. In fact, what should be used in the IMF of equation (1) is the initial mass M of the progenitor of a clump star with mass $M_{\rm cl}$. $M - M_{\rm cl}$ is however always less than 0.2 $M_{\odot}$ for the case of Reimers' mass-loss with $\eta = 0.4$[1]. Thus, for the illustrative purposes we are interested in this moment, we prefer to ignore this effect and simply adopt the Salpeter IMF in Fig. 1.

The third panel from top to bottom shows the CHeB lifetime as a function of $M_{\rm cl}$. As remarked in Girardi & Bertelli (1998) and Paper I, this lifetime increases for stars with lower core masses $M_{\rm c}$ at the moment of He-ignition, i.e. those in the vicinity of $M_{\rm Hef}$. This is so because the lower the initial core mass in the CHeB phase (see upper panel of Fig. 1), (i) the more nuclear fuel becomes available for the H-burning shell, and (ii) the lower is the luminosity at which CHeB takes place (middle panel of Fig. 1).

Finally, the bottom panel of Fig. 6 presents the final mass distribution $N(M_{\rm cl})$ [from equation (1)] for a galaxy model in which the SFR is assumed to be constant over the complete age interval up to 10 Gyr. The maximum age of 10 Gyr implies the cut-off in this distribution along the vertical line at $M_{\rm cl} = 0.9\ M_{\odot}$. An important aspect evidenced by this figure is that *the mass distribution of clump stars has a second maximum at $M \simeq M_{\rm Hef} = 2\ M_{\odot}$*. Moreover, *the CHeB stars with mass slightly higher than $M_{\rm Hef} = 2\ M_{\odot}$ are not severely under-represented with respect to lower-mass ones.* In the particular case here shown, the number ratio between stars with $M_{\rm cl} \geq 2\ M_{\odot}$ and those with $2 > (M_{\rm cl}/M_{\odot}) > 0.9$ is of 0.19. Moreover, it can be noticed that clump stars with mass higher than about $M_{\rm cl} \gtrsim 2.5\ M_{\odot}$ become very few, due to the reduction of both their lifetimes and representativeness in the IMF.

4.2. The secondary clump in different galaxy models

The CHeB stars with mass close to $M_{\rm Hef}$ are not only relatively frequent (bottom panel of Fig. 6), but are also located into a particular region of the HR diagram (see Fig. 1). They are up to 0.4 mag fainter than the slightly less-massive and older clump stars. Also, in metal-rich stellar populations they are the bluest among clump stars. Due to these characteristics, they can define a *secondary clump* in the CMD.

This feature was predicted in Paper I, and identified with a small group of stars in the *Hipparcos* CMD of nearby stars (see Figs. 2, 3 and 4 therein). The reader is referred to that work for a generic description of this point. Suffice it to recall here that this feature corresponds to the approximate position of the 2 $M_{\odot}$ track in Fig. 2. The main red clump would correspond to CHeB stars in the mass range from about 1.9 to 0.9 $M_{\odot}$.

In Fig. 7, we make use of synthetic CMDs in order to predict how the red clump looks at different metallicities. This in the ideal cases in which the star formation has proceeded at a constant rate and with a constant value of mean metallicity. The models include also a small Gaussian dispersion of metallicities, of $\sigma_Z/Z = 0.1$, and the effect of mass loss along the RGB. The method of synthesis here used is the same as in Paper I, and takes into account all stars in all evolutionary stages, with all ages and metallicities, which can be contributing to each point of a given CMD.

The plots for the highest metallicities show red clumps covering a considerable range in colour. This colour dispersion may be interpreted as an age sequence, with younger (more massive) clump stars having bluer colours. At the extreme left of this sequence, the clump luminosity decreases by about 0.4 mag. This region of the CMD is identified with the secondary clump we refer. It corresponds to a real increase in the stellar density, as can be seen from the contour plots in Fig. 7. Moreover, in Section 4.3 below we argue that this feature should become even denser (i.e. more clumpy) if we further improve the mass resolution of our stellar models.

It is also clear from this plot that the red clump is expected to be narrower in colour for lower metallicities. Moreover, in the diagrams for $Z = 0.001$ (which may well illustrate the typical case for Pop. II), the low-mass (and hence oldest) tail of the clump is already bending to the blue, and then partially superimposes on the region which would correspond to the secondary clump. As a consequence, the latter becomes almost undistinguishable from the main clump. Both could not be separated in real CMDs with some realistic distribution of photometric errors. On the contrary, in stellar populations of higher metallicity, the secondary clump clearly separates from the main one. We can conclude that *the secondary red clump is well separated from the main one only at metallicities higher than about* $Z = 0.004$. For lower metallicities, all clump stars with masses higher than about 0.7 $M_{\odot}$ may be mixed into a single clump feature.

[1] It can be noticed from the upper panel of Fig. 6: for a given age, the mass difference between the two drawn lines (dashed minus continuous) gives a good estimate of the mass lost by each star in the RGB, $M - M_{\rm cl}$.

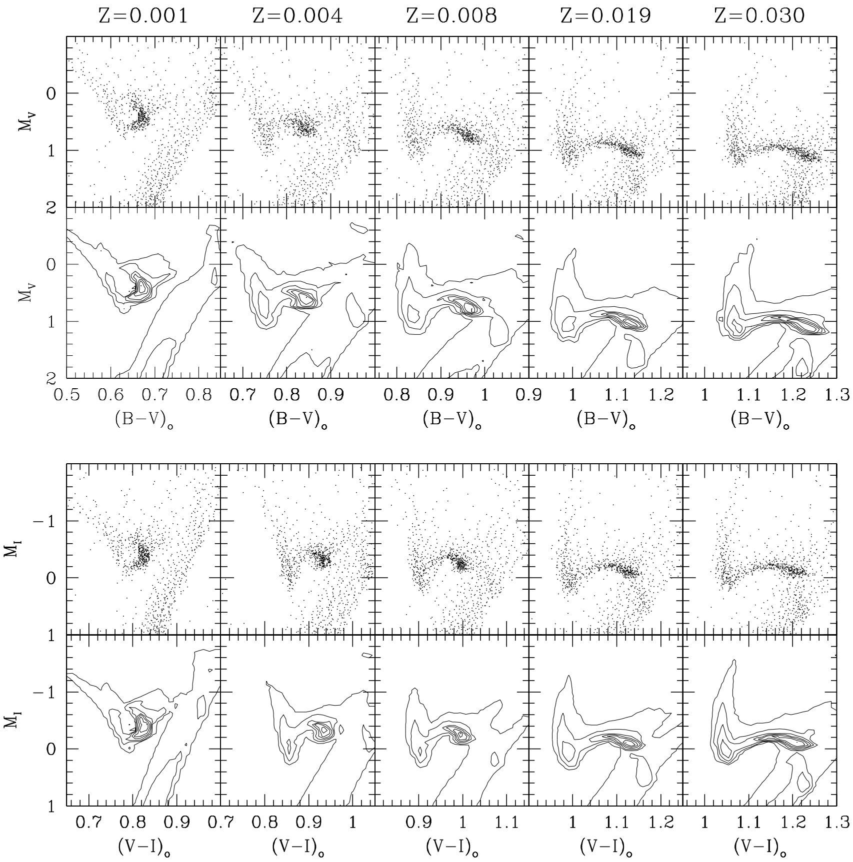

Fig. 7. Synthetic CMDs showing the red clump region for different metallicities, in the BV (top panels) and VI (bottom ones) planes. Each simulated CMD is presented in two versions: in the first one, 6 contour lines limit regions with the same stellar density N, and are spaced at constant intervals of $N^{1/2}$. Immediately above, we show the corresponding synthetic CMD for a total of 1000 stars. Models assume constant SFR from 0.1 to 10 Gyr, constant mean metallicity, and a small metallicity dispersion (see text). Panels from left to right are for mean metallicities $Z = 0.001$, 0.004, 0.008, 0.019, and 0.03. The most densely populated region of the diagrams represent the main body of the red clump. To its blue, we have the structure which contains both the faint secondary clump and the plume of brighter clump stars. The RGB runs slightly to the red of the main clump. It presents another concentration of stars (more evident in the right-hand panels), which corresponds to the RGB bump.

Of course, the case of constant SFR and metallicity is illustrative, but not representative of most galaxy fields. In Paper I we presented a synthetic CMD of stars in the solar vicinity, in which an age–metallicity relation was assumed, together with an age-dependent factor to account for the fact that older stars are located at larger heights above the galactic plane. Also in that case a secondary clump was present in the models, and yet clearly separated from the main clump.

In Fig. 8 we show another simulation for a galaxy following an age-metallicity relation. In this model, the SFR is assumed to be exponentially decreasing with the galactic age, with an e-folding time of 5 Gyr. Then we adopt the metallicity evolution predicted by the simple closed-box model of chemical evolution (Searle & Sargent 1972): Z increases linearly with time, from a minimum value of $Z = 0.001$ at 12 Gyr ago, to the present value of $Z = 0.019$. The result is that the main red clump becomes a feature very extended in colour. The secondary red clump is however still present, at a colour corresponding to that of the 1 Gyr old population [ie. at $M_V \simeq 1.1$, $(B-V)_0 \simeq 0.97$ in the top panels, and at $M_I \simeq 0.1$, $(V-I)_0 \simeq 0.98$ in the bottom panels], but superimposed on the RGB of the more metal-poor populations. In an observed CMD, such a feature could hardly be distinguished from the background of RGB stars. Moreover, we can also observe that other faint concentrations of stars come out along the RGB and slightly below the

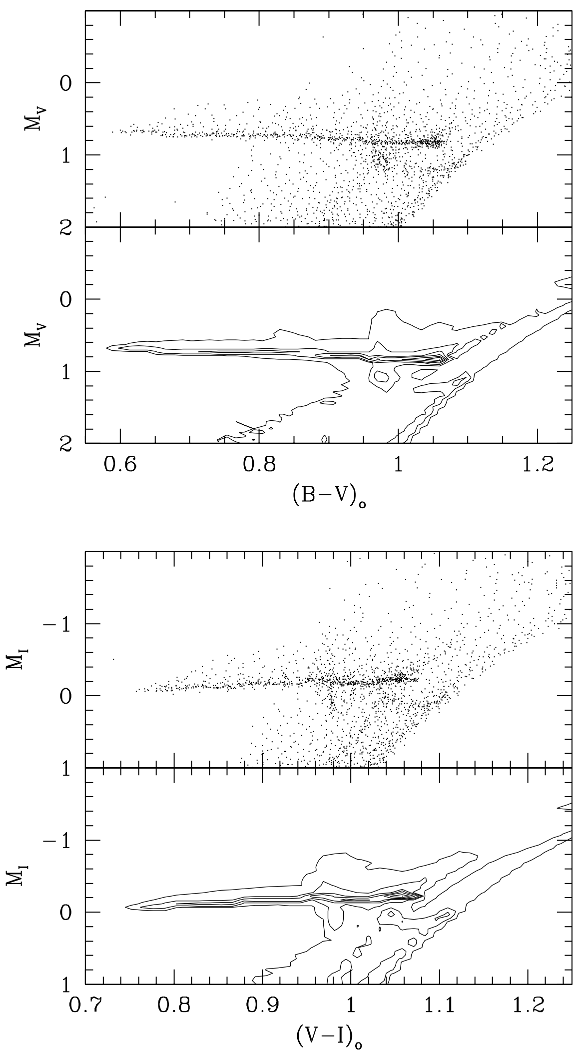

Fig. 8. Synthetic CMDs showing the red clump for a galaxy model which assumes a simple chemical evolution history, in the BV and VI planes. The different panels are as in Fig. 7. The synthetic CMDs include a total number of 2000 stars. The model assume a exponentially decreasing SFR from 0.1 to 12 Gyr, and a metallicity linearly increasing with the galaxy age (see the text for details).

main clump; they correspond to the RGB bump of metal-rich stellar populations, and should not be confused with the secondary clump of CHeB stars. Finally, the reader is invited to compare these synthetic CMDs with that of the M 31 field presented by Stanek & Garnavich (1998, their figures 2 and 4). Such a comparison evidences the capability of the present models of reproducing the general features of the M 31 clump, especially in regard to its colour range and inclination in the M_I vs. $V-I$ diagram.

The case of galaxy populations with large metallicity dispersions at a given age are not presented here. The properties of the corresponding clumps are however easy to derive from the above plots. Since the secondary clump is in general less populated than the main one, a large metallicity dispersion at 1 Gyr would make it to become a feature of lower density, and therefore not easily distinguishable from the background population of RGB stars present in most CMDs.

In the case of a constant SFR, the total number of low-mass clump stars is basically determined by the maximum age T of the stellar populations we consider. For $T = 10$ Gyr, we have a lower mass limit of 0.9 $M_\odot$, which is increased to 1.3 $M_\odot$ if we adopt $T = 4$ Gyr. Thus, in the case of relatively young galaxies, the number ratio between the stars with $M_{\rm cl} > M_{\rm Hef}$ and those with $M_{\rm cl} < M_{\rm Hef}$ increases (see e.g. the bottom panel of Fig. 6). This circumstance would make *the secondary clump more evident, when compared to the main clump, in galaxies which have increased their SFR in the last Gyr or so of their evolution.*

4.3. On the mass range and resolution of the clump models

The secondary clump can also be interpreted as being the faint extremity of a large vertical structure in the CMD, i.e. the sequence of CHeB stars which ignited helium in non-degenerate conditions. The brightest part of this sequence consists of a plume of stars departing from the main red clump to higher luminosities. It has been noticed in the CMD of several Local Group galaxies (e.g. Zaritsky & Lin 1997; Beaulieu & Sacket 1998; Alves et al. 1998; Tolstoy et al. 1998), and is often referred to as the 'vertical red clump' or 'blue loop feature'. This feature is also evident in the simulations of Fig. 7.

But how could the secondary clump have been missed in previous studies of synthetic CMDs, contrarily to this less populated bright tail? A crucial aspect here regards the mass resolution of the grids of evolutionary tracks used to construct synthetic CMDs. In Paper I, we made use of grids with a resolution of $\sim 0.1\ M_\odot$ in the vicinity of $M_{\rm Hef}$. These closely spaced tracks allowed the construction of accurate isochrones even for this mass (and hence age) interval in which the evolutionary features change so remarkably.

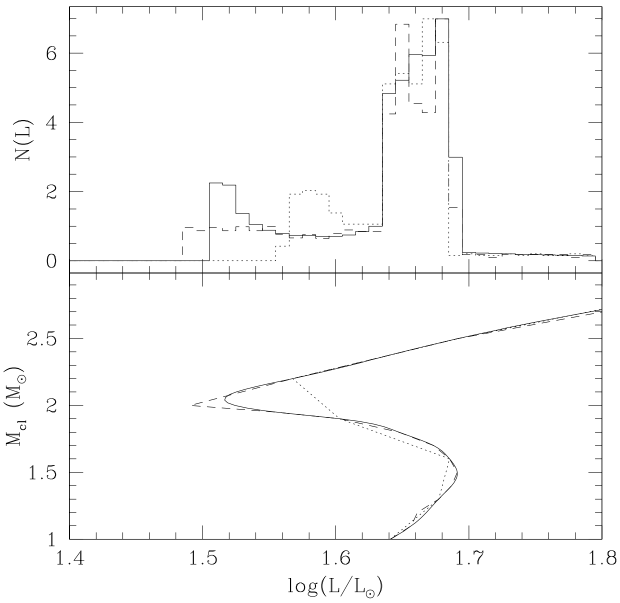

Fig. 9. Lower panel: $L_{\rm cl}(M_{\rm cl})$ relations as obtained from grids of evolutionary tracks computed with different mass resolutions: $\Delta M_{\rm cl} = 0.3\ M_\odot$ for the dotted line, $\Delta M_{\rm cl} = 0.1\ M_\odot$ (typically) for the dashed line, and the idealised case of $\Delta M_{\rm cl} \to 0$ for the continuous line. Upper panel: The luminosity functions of clump stars as derived from these sequences, in arbitrary units. Notice the different characteristics of the fainter clump in the three cases.

To give a better idea of the importance of having a dense grid of tracks in order to find the secondary clump, Fig. 9 shows simple simulations of the luminosity distribution obtained from stellar models at the stage of lowest luminosity during the CHeB (i.e. ignoring the remaining CHeB evolution), calculated with different mass resolutions. In these simple models, equation (1) gives the number of stars to be assigned to each mass bin $[M_{\rm cl}, M_{\rm cl} + \Delta M_{\rm cl}]$, with a constant luminosity distribution over the corresponding luminosity bin $[L_{\rm cl}, L_{\rm cl} + \Delta L_{\rm cl}]$ (see bottom panel). The contributions from the stars in the complete mass interval from 1 to 3 $M_\odot$ are summed in order to construct the luminosity functions shown in the upper panel.

All the simulations in Fig. 9 clearly show a main clump at $1.64 < \log(L/L_\odot) < 1.70$ (upper panel), corresponding to the ZAHB stars with $1.0 < M_{\rm cl}/M_\odot < 1.8$ (see bottom panel), and a second feature located at a somewhat fainter luminosity. In the case with the worst mass resolution ($\Delta M_{\rm cl} = 0.3\ M_\odot$; dotted line), the minimum of luminosity for CHeB stars with $M_{\rm cl} = M_{\rm Hef}$ is missed, and therefore the resulting secondary clump is located only 0.06 dex in luminosity (0.15 mag) below the main one. If we then were to consider the excursion of $\lesssim 0.3$ mag upwards in luminosity during the stellar CHeB evolution in these models, the faint feature would be blurred enough to be mixed with the main red clump.

However, as we improve the mass resolution of the models, the secondary clump emerges at lower luminosities. The dashed line shows the clump as derived from our CHeB sequences, for which $\Delta M_{\rm cl}$ is of typically 0.1 $M_\odot$. In this case the faint extension of the red clump becomes a more extended feature in the luminosity function, defining a second maximum ~ 0.14 dex (0.35 mag) below the main one. This maximum is however not very pronounced.

The continuous line instead shows the ideal situation of a continuous and smooth CHeB sequence (see bottom panel), in order to simulate the $\Delta M_{\rm cl} \to 0$ case. This line was obtained from a natural cubic spline passing through most (but not all) of the computed model points. In this case, the minimum of the $L_{\rm cl}(M_{\rm cl})$ function defines a caustic in the luminosity distribution, which causes the faint secondary clump to become a quite striking feature, clearly separated in luminosity from the main clump by a gap of 0.35 mag. In this case, the excursions in luminosity during the CHeB evolution would not be enough to blur this feature with the main red clump.

Sweigart, Greggio & Renzini (1989, 1990) computed evolutionary tracks of hydrogen burning stars up to the He-ignition, with a very fine mass resolution, of 0.05 $M_\odot$ close to $M_{\rm Hef}$. These models are especially suited to study the velocity at which the RGB appears in aging stellar populations. The functions $M_{\rm cl}(M)$ they derive (Sweigart et al. 1990) are indeed very smooth along the transition from low- to intermediate-mass stars. Even if they do not compute the subsequent He-burning evolution from these tracks, their $M_{\rm cl}(M)$ relations clearly suggest $L_{\rm cl}(M)$ functions behaving similarly to the spline curve shown in Fig. 9. This behaviour is also the expected one since stars in the transition region, with mass close to $M_{\rm Hef}$, ignite helium at different degrees of electron degeneracy. These results, and the simple exercise presented in Fig. 9, leads us to conclude that *the secondary clump shall be even more pronounced than found in models with 0.1 $M_\odot$ resolution.*

Apart from the mass resolution, another point of concern is the internal consistency of the stellar tracks computed. In the present models, the core mass at the ZAHB phase is assumed equal to that at the onset of the He-flash on the RGB, as well as the envelope chemical composition. The only effect of the He-flash is assumed to be the conversion of 5 percent of the helium core mass into carbon. Instead, tracks computed under the assumption of a constant core mass for all ZAHB models of low-mass stars would fail to produce the decrease in the clump luminosity as we approach $M_{\rm Hef}$ (see Fig. 1), and hence fail to describe the details of the secondary clumps. On the other hand, models which follow the complete stellar evolution during the He-flash in a self-consistent way, would probably give an even better description of the $M_{\rm Hef}$ transition region than the present ones.

4.4. Observations of the secondary clump

Is the secondary red clump observed in real stellar populations? Paper I presents a discussion of the local clump defined by *Hipparcos* data. In that work, the great similarity between the predicted and observed CMDs immediately suggested the presence of the secondary clump in the data (see figures 2, 3 and 4 in Paper I). The two only visual binaries located in the 'secondary clump region' of the *Hipparcos* CMD and with reliable orbital parameters, resulted to have primary stars with masses consistent with the prediction that they should be close to $M_{\rm Hef} \simeq 2\ M_\odot$ (see also Section 4.6 below).

Bica et al. (1998) recently presented CMDs in the Washington system for several clusters and surrounding fields in the LMC. In two of the fields in the northest part of this galaxy, close to the clusters SL 388 and SL 509, a striking secondary clump was observed *about 0.45 mag below the dominant intermediate-age clump, and at its blue side.* The same feature was present in a third field, SL 769, located closer to the LMC bar and many degrees away from the above-mentioned ones.

The authors tentatively suggested that the second clump could be the signature of a tidal arm or dwarf galaxy located about 10 kpc beyond the LMC, at a distance similar to the SMC. Of course, the present models raise the possibility that the secondary, fainter clumps are simply caused by a younger stellar population inside the LMC. The reader is invited to compare the simulations of the LMC clump presented in the figure 9 of Paper I (and also in Girardi 1998), with the observed CMDs shown in figure 4 of Bica et al. (1998). These diagrams are not completely equivalent: the Paper I models are presented in the M_I vs. $V-I$ plane, while the latter observations are presented in the T_1 vs. $C-T_1$ plane of Washington photometry. Apart from the use of these different systems, the modeled clumps are remarkably similar to those observed in the SL 388 and SL 509 fields.

But how could this secondary clump be observed only in some of the LMC fields? To answer this question, let us recall the conditions for its appearance in a CMD:

1. The observed field should contain a significant number of stars about 1 Gyr old, and hence with $M_{\rm cl} \sim 2\,M_{\odot}$, mixed to a population of older stars.
2. The 1 Gyr old population should not be too dispersed in colour due to its intrinsic metallicity dispersion. The bulk of clump stars should be more metal-rich than about $Z = 0.004$.
3. Both main and secondary clumps should not be mixed together due to effects such as differential reddening, distance dispersions, and photometric errors. The combination of these effects should be producing r.m.s. dispersions lower than about 0.2 mag in the apparent magnitudes of clump stars.

Hubble Space Telescope (HST) observations generally include too few clump stars to comply with item 1. On the contrary, ground-based observations can easily sample large numbers of clump stars, but in general present the problems referred to in item 3. Moreover, many galaxy fields are expected not to comply with item 2. Therefore, it is no surprise that the secondary clumps have not been noticed for so long. The bimodal clumps observed by Bica et al. (1998) may be the signature of regions with an unusually large population of 1 Gyr old stars, and/or with unusually small dispersion of reddening. In fact, the SL 388 and SL 509 fields are located in the outer parts of the LMC disk, about $5^{\rm o}$ away from the bar. In these regions, the reddening internal to the LMC should be very small, as well as its dispersion.

Moreover, the dual clump observed in the field of SL 509 is found to be present in the cluster itself, with the fainter clump this time being more pronounced than the bright one (Bica et al. 1998). It is then interesting to consider the age of this cluster. Its integrated UBV colours ($B-V = 0.73, U-B = 0.19$; Bica et al. 1996) indicate an S-parameter of 41 (see Elson & Fall 1985; Girardi et al. 1995), which is equivalent to an age of $\log(t/{\rm yr}) = 9.22 \pm 0.23$ ($1.66^{+1.15}_{-0.81}$ Gyr), according to the S-age calibration of Girardi et al. (1995; eq. 5 therein). On the other hand, Bica et al. (1998) derive an age of 1.2 Gyr for SL 509, based on a calibration between the magnitude difference from the turn-off to the red clump, δT_1, and the age (Geisler et al. 1998). In this age range, however, δT_1 is expected to become less sensitive to age due to the leafting of core degeneracy, which causes the clump to have magnitudes similar to the turn-off. Nonetheless, δT_1 provides a firm upper limit to the age of the cluster, which we estimate as being of 1.5 Gyr. Thus, the age of this cluster is probably comprised between 0.85 and 1.5 Gyr, which is consistent with the idea that it contains evolved stars just massive enough for having ignited helium in non-degenerate conditions. SL 509 is then probably similar to the cases NGC 2209 and NGC 2190 indicated in Fig. 3.

We conclude that the *Bica et al. (1998) data provides consistent evidence for the existence of the secondary clump in the LMC field population.* Of course, the question arises whether the same feature can be identified in other previously published CMDs as well. Some CMDs indeed present clumps with faint extensions which are compatible with the characteristics of the secondary clump predicted by theory: e.g. the HST data of Holtzmann et al. (1997, their figure 2), Sarajedini (1998, their field WF2 in figure 4) and Smecker-Hane et al. (1998), the VR photometry of Beaulieu & Sackett (1998, their least crowded field F2), and the VI of Stappers et al. (1997, their figure 1). In none of these cases however the secondary clump is as striking to the eye as in Bica et al. (1998) data. A particularly unfortunate circunstance is that most authors (including those listed above) present CMDs in which the V or F555W magnitudes are in the abcissa, whereas the secondary clump would be better separated from the main one if redder pass-bands were used instead.

In Fig. 10 we present a comparison between our models and the Geha et al. (1998) HST WFPC2 data for two particular LMC fields (see also Holtzmann et al. 1997). The right panel presents the F814W vs. F555W−F814W CMD from the combined LMC fields referred to as F1 and F2 in Geha et al. (1997, see their table 1). We recall that the HST filters F555W and F814W are roughly equivalent to the V and I ones.

The left panel presents the synthetic M_I vs. $V-I$ CMD for a model produced by the sum of two different components: (i) the first one has a constant SFR over the age interval from 0.1 to 3 Gyr ago, with a gaussian distribution of metallicities of mean $Z = 0.008$ and dispersion $\sigma_Z = 0.002$; whereas (ii) the second one presents a 5 times lower SFR from 3 to 10 Gyr ago, with a mean $Z = 0.004$ and dispersion $\sigma_Z = 0.002$. This particular model is by no means a careful attempt in order to describe the data; it is just meant to be a synthetic CMD which reasonably resembles the observed one, especially in the region of the subgiants and red giants.

What is most remarkable in this figure is the similarity between the clumps in both panels, which clearly span a range in magnitude of about 0.6 mag. In the simulation, this width is caused mainly by the presence of the secondary clump. In the data, the photometric errors at the clump level are simply neglegible (of ~ 0.03 mag, see figure 3 in Holtzmann et al. 1997), which is probably also the case for the dispersion in the internal reddening. Therefore, the observed clump width cannot be accounted by these factors. Instead, we regard *the intrinsic clump structure, as suggested by the models, as the simplest explanation for the large clump width observed in these LMC fields.*

Mermilliod et al. (1998) recently reported another very interesting observation: a dual clump is present among the members of the open cluster NGC 752. The brighter clump is composed of 8 stars, whereas the fainter and bluer one contains 3 or 4 stars. Moreover, this cluster has an age close to the limit for having non-degenerate helium ignition (see

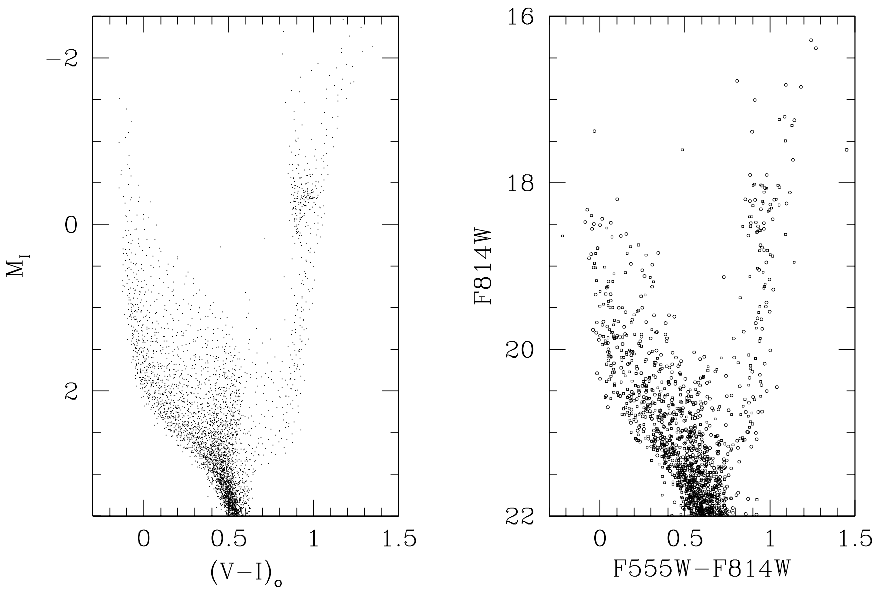

Fig. 10. Comparison between a synthetic CMD (left panel) and the HST data for the LMC field (right panel). The simulation contains 5000 stars, distributed according to the model described in the text. The data corresponds to the fields F1 (squares) and F2 (circles) studied by Holtzmann et al. (1997) and Geha et al. (1998).

e.g. Daniel et al. 1994; Carraro & Chiosi 1994). Therefore, we face the interesting possibility of observing a cluster at the right age to contain both the clump stars which went, and those which did not went, through the helium flash. We remark that the probability of finding such a cluster is somewhat low, because of the narrow range of initial masses typically covered by the clump stars in individual clusters. On the contrary, dual clumps should be frequent in galaxy fields.

4.5. The secondary clump as a tracer of the star formation history

The secondary red clump is a CMD feature sensitive to the history of star formation in the parent galaxy field. A good example of this may be found in the LMC. Indeed, most studies of the field population indicate that the LMC disc is relatively young on average, having formed a large fraction of its stars (if not most) in the last 4 Gyr or so (see e.g. Bertelli et al. 1992; Vallenari et al. 1996; Holtzmann et al. 1997; Geha et al. 1998). This circunstance may contribute to make the secondary clump in this galaxy particularly strong if compared to the older, main clump.

Models like the one presented in Fig. 10 suggest that the number of stars in the secondary clump feature should be simply proportional to the SFR at the age of 1 Gyr. In fact, this CMD feature is expected to be an excellent tracer of the spatial distribution of star formation in the LMC at ~ 1 Gyr ago. Hence, *it would be extremely interesting to check the available photometric data* (e.g. in the EROS, MACHO, OGLE, and Magellanic Cloud Photometric Survey databases) *in order to identify the secondary clump in different fields of the LMC*, and hence possibly to map its SFR at 1 Gyr ago. Of course, the same comments apply to all Local Group galaxies for which high-quality and uncrowded stellar photometry is feasible.

The number ratio between stars belonging to the main and secondary clumps, is affected by both the IMF and the particular details of the SFR history over a much longer age interval, from 1 Gyr to $12-15$ Gyr. Thus, this number ratio does not provide an unique interpretation in terms of the SFR. The study of the complete CMD would be necessary to this aim. We remark, however, that *the observed clump structure can provide additional constraints (which have so far been neglected) for the derivation of the SFR history in galaxy fields.*

4.6. Measuring $M_{\rm Hef}$ with stars in the secondary clump

Figure 9 shows that stars in the secondary clump should have masses close to $M_{\rm Hef}$. More specifically, for a single value of metallicity, stars more than 0.2 mag below the main red clump have masses contained within the relatively narrow interval of $[M_{\rm Hef}+0.2M_{\odot}, M_{\rm Hef}-0.1M_{\odot}]$.

The limiting mass $M_{\rm Hef}$ (Section 2) is sensitive to the adopted chemical composition, and to the treatment of the convective boundaries of the core during the main sequence phase. The upper panel of Fig. 1 and Table 1 illustrate how its value gets lower for lower values of metal and helium content. The values we get (e.g. $M_{\rm Hef} = 2.0\ M_{\odot}$ for $Z = 0.019$) are typical of models computed with a moderate amount of convective overshooting. We computed an additional set of $Z = 0.019$ tracks adopting the classical Schwarzschild criterion for the boundary of convective regions, obtaining $M_{\rm Hef} = 2.4\ M_{\odot}$. Our values agree, to within 0.1 $M_{\odot}$, to those found by different authors in models of similar characteristics (Sweigart et al. 1990; Maeder & Meynet 1989; Bertelli et al. 1994, and references therein).

These considerations led us to suggest, in Paper I, *the use of secondary clump stars located in binary systems in order to observationally constrain* $M_{\rm Hef}$. The mass information from the binary orbit, together with some measure of the stellar metallicity, could allow to get a direct measure of $M_{\rm Hef}$, and hence constraints on the efficiency of convective overshooting in stellar cores.

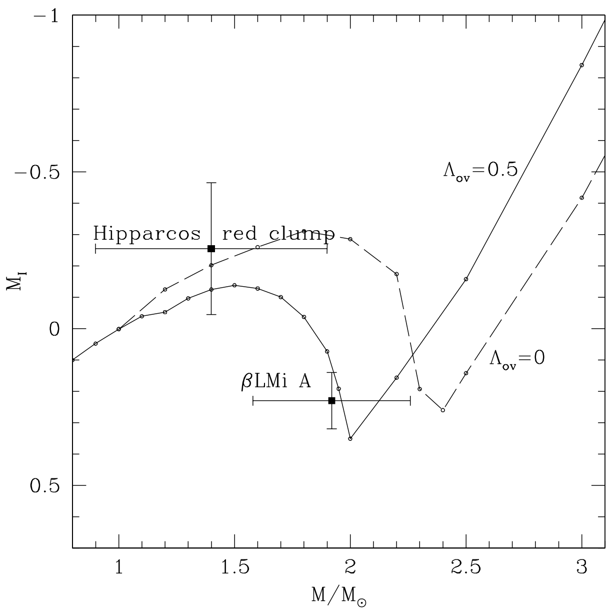

Fig. 11. The I-band absolute magnitude of clump stars as a function of their mass, for solar metallicity. The lines delimit the lower boundary of the clump as predicted by models with and without overshooting (solid and dashed lines, respectively). The mean position of the Hipparcos clump, and of the β LMi primary star, are also presented. The position of β LMi in this diagram indicates a star just massive enough for having ignited He in non-degenerate conditions, and would favour the case of moderate convective overshooting.

Figure 11 illustrates the most favorable case we find in the *Hipparcos* catalog of binary stars (ESA 1997). It regards the visual binary β LMi (HD 90537), which has well-measured orbital parameters (Heintz 1982) and an uncertainty in *Hipparcos* parallax of 4 percent. The primary star, with a derived mass of $1.92 \pm 0.34\ M_{\odot}$, probably belongs to the secondary clump defined in the CMD from *Hipparcos* (see Paper I). Its spectrum indicates [Fe/H] = 0.0 (McWilliam 1990), i.e. solar metallicity. In the figure, we show the M_I absolute magnitude as a function of mass for the lowest-luminosity CHeB models of $Z = 0.019$ (cf. Fig. 1), for both the classical ($\Lambda_{\rm c} = 0$) and moderate overshooting ($\Lambda_{\rm c} = 0.5$; see Alongi et al. 1993; Chiosi et al. 1992, and references therein) cases. The mean position and dispersion of the *Hipparcos* red clump is indicated by error bars. Similarly, we plot the probable position of the primary star β LMi A with the corresponding standard errors. Assuming that this star is in the stage of CHeB (as its position in the *Hipparcos* CMD indicates), its measured mass would be consistent with a value of $M_{\rm Hef} \simeq 1.9\ M_{\odot}$, and would favour the case of moderate convective overshooting as indicated by the $\Lambda_{\rm c} = 0.5$ line.

Of course, no firm conclusions about the efficiency of convective overshooting can be taken from a single star, for which the parameters are not known with the desired accuracy. We have further checked the data for well-studied visual binaries in the solar vicinity, finding no better candidate to belong to the secondary clump. Future or alternative data may improve upon this result.

4.7. The red clump as a distance indicator

There are two ways in which the red clump can be used as a distance indicator. The first one has been commented on in Section 1, and regards the *absolute distance determinations* of Local Group galaxies. It relies on the clump absolute magnitude $M_I^{\rm cl}$ as measured from local stars in the *Hipparcos* database, and on the assumption that it is constant for different galaxies. The result on a very short distance to the Magellanic Clouds (Udalski et al. 1998; Stanek et al. 1998) caused the suspicion that systematic effects could be present in the method. Cole (1998) and Paper I identified the dependence of the clump absolute magnitude with age and metallicity, suggested by the models, as the main responsible for the discrepant results for the Clouds. Additionally, Gratton, Carretta & Clementini (1998) call attention to the large values of the absorption A_I to the Clouds used by Udalski et al. (1998) and Stanek et al. (1998). If more conservative values of A_I and the metallicity-age corrections to $M_I^{\rm cl}$ are adopted, the LMC distance as derived from the red clump can yet be reconciled with the more traditional values of $(m-M)_0 = 18.5 \pm 0.1$ mag. Clearly, the red clump stars alone do not provide a definitive value to the LMC distance modulus.

Comparing the clump and RR Lyrae data for fields in the LMC, SMC, and Carina dwarf galaxy, Udalski (1998a) try to access the dependence of $M_I^{\rm cl}$ on metallicity, concluding that it varies very little, i.e. $M_I^{\rm cl} = (0.09 \pm 0.03)\,[{\rm Fe/H}]+$ constant. However, this conclusion largely holds on the assumption that the RR Lyrae in the observed fields provide accurate standard candles, and that the RR Lyrae absolute magnitudes vary with metallicity as $M_V = (0.18 \pm 0.03)\,[{\rm Fe/H}] +$ constant. At least the second point may be considered as controversial (see eg. Gratton et al. 1998; Popowski & Gould 1998).

Udalski (1998b) also attempt to derive the dependence of $M_I^{\rm cl}$ on the age of Magellanic Cloud clusters, limiting the analysis to the age interval from 2 to 15 Gyr. His data has been discussed in Section 3.1. Considering the undertainties on the reddening and distances for individual star clusters, Udalski's (1998b) data is consistent with the behaviour of clump magnitudes predicted by models (Fig. 4). Udalski (1998ab) instead refers to the models as 'involving many difficult to verify and often controversial assumptions like mass-loss, helium content, star formation rate, etc'. We would like to stress that uncertainties in the mass-loss rates play a negligible role in determining the clump structure in the local *Hipparcos* sample and in the LMC. This is so because all stars with $M > 1.5\,M_\odot$ suffer from negligible mass-loss along the RGB. Only the reddest tail of these clumps may be slightly affected by mass-loss, which would however not change appreciably the derived clump mean magnitudes. On the other hand, the helium-to-metal content relation adopted in the present models, $Y(Z) \simeq 0.23 + 2.25\,Z$ (see Table 1 for the precise Y values), represents a fairly conservative one. Independent of these assumptions, the models are quite clear in indicating a dependence of the clump I-band absolute magnitude on metallicity, a point which is crucial to the method of distance determinations based on clump stars.

One of the main uncertainties in the models, for instance, may be identified in the adopted transformations from the theoretical to observational planes (bolometric corrections and $T_{\rm eff}$–colour relations, e.g. Kurucz 1992). Inadequacies in these tranformations are able to systematically shift models in their colours and absolute magnitudes. But since these are probably *mostly systematic* errors, they cannot significantly affect the relative values between these quantities as derived from models. The metallicity dependence of $M_I^{\rm cl}$, for instance, largely reflects the dependence of $\log(L/L_\odot)$ on this parameter (see Fig. 1), and not the bolometric corrections.

The magnitude distribution of the red clump has also been used as a *relative distance indicator*. Hatzidimitriou & Hawkins (1989), Gardiner & Hawkins (1991) and Gardiner & Hatzidimitriou (1992) have used the width of the luminosity function of red clump stars in different regions of the SMC, in order to map its depth along the line-of-sight. For some regions, the clumps were observed to be very narrow in magnitude, with standard widths of about $\sigma = 0.1$ mag. On the other hand, other regions presented clump widths of up to $\sigma = 0.5$ mag. These broad clumps were interpreted as being the signature of different stellar populations located at different distances. This assumption lead to the derivation of depths of the SMC populations along the line-of-sight, which range from $4-6$ to $12-16$ Kpc in different regions of the SMC (Gardiner & Hawkins 1991).

The present models instead indicate that the red clump is not intrinsically narrow in all situations. In the particular cases of metal-poor galaxy fields with a constant SFR, for instance, the red clump is expected to have an intrinsic width of at least $\sigma = 0.2$ mag (see e.g. the left panels of Fig. 7). Slightly larger intrinsic widths may be present if the star formation has been particularly intense at 1 Gyr ago (see e.g. Fig. 10), due to the appearance of the secondary clump. In this case, the increased clump width is expected to correlate with the presence of a larger population of main sequence stars nearly as bright as (or even brighter than) the clump level in the CMD. Moreover, additional broadening of the clump is expected when a field presents a significant metallicity dispersion.

Therefore, part of the observed clump width in the SMC may possibly be interpreted as intrinsic variations of the clump absolute magnitude, rather than the inferred depth structures. The same comment apply as well to the LMC population. A re-evaluation of the Magellanic Clouds clump data may be of interest in order to clarify these points. We remark, however, that the kinematical data of Hatzidimitriou, Cannon & Hawkins (1993) seem to confirm the presence of different structures along the SMC line-of-sight, at least in the areas of maximum inferred depth.

Another example of the use of the clump as a relative distance indicator is the work by Zaritsky & Lin (1997). Having identified a brighter extension of the LMC clump (up to $\sim$ 1 mag wide), they suggested it should be caused by an intervening stellar population located between us and that galaxy. This would have important implications to the interpretation of the observed rate of micro-lensing events towards the LMC. However, Beaulieu & Sackett (1998) and Ibata, Lewis & Beaulieu (1998) convincingly argued that this 'vertical red clump' should rather be caused by the youngest red clump stars (see also Sects. 4.2 and 4.4 above). This further illustrates that the red clump should be used with care in distance determinations, and that synthetic CMDs may be of invaluable help in the analysis of similar data. Moreover, it evidences that intermediate-mass stars cannot be neglected in the modelling of the red clump.

5. Concluding remarks

The main results of the present work may be summarized as follows:

1. Present data about the clump magnitude in Magellanic Cloud clusters are consistent with the behaviour predicted by stellar evolutionary models. Particularly interesting is the presence of a minimum in the luminosity of clump stars for an age of about $\sim$ 1 Gyr, clearly evidenced by the Corsi et al. (1994) data, which corresponds to the maximum age for stars which ignite helium under non-degenerate condictions. The presence of this luminosity minimum is therefore a solid theoretical prediction. This minimum occurs for stars with mass $M_{\rm Hef} = 2.0\ M_\odot$ if the metallicity is about solar and moderate convective overshooting is assumed. In models without convective overshooting, it would rather correspond to ages of about 0.5 Gyr, and stellar masses of about 2.4 $M_\odot$.
2. The same stellar models are used to generate synthetic CMDs for different galaxy fields. It turns out that these models predict the presence of a secondary red clump in the CMD, which is located about 0.4 mag below the main clump, and slightly to its blue. This feature is expected to be present in fields which formed stars $\sim$ 1 Gyr ago, and in which the typical metallicities are higher than about $Z = 0.004$.
3. In order to describe well this feature in synthetic CMDs, stellar evolutionary tracks should be computed with a fine mass resolution in the complete relevant mass interval, i.e. from the lowest possible mass of clump stars, up to about $M_{\rm Hef} + 0.5\ M_\odot$. In the vicinity of $M_{\rm Hef}$, a mass resolution of at least $\Delta M = 0.1\ M_\odot$ is required. Moreover, this work evidences that the mass interval of $M_{\rm cl} \gtrsim M_{\rm Hef}$ may represent a significant fraction of the clump stars. Therefore, it cannot be neglected in detailed studies of the red clump, especially in regard to galaxies that have kept forming stars in the last few gigayears of their evolution.
4. Secondary clumps consistent with the model predictions are present in *Hipparcos* CMD for nearby stars, and in some LMC fields observed by Bica et al. (1998). Similar features are present, although not too clear, in LMC data presented by several other authors. Secondary clumps may be missing or hidden in the CMDs of other galaxy fields due either to the poor number statistics, or to a large dispersion in reddening and metallicity, or to photometric errors, or to the absence/scarcity of 1 Gyr old populations. Data for fields in the Magellanic Clouds and other Local Group galaxies should be carefully re-investigated in the light of these results. In fact, this fine structure of the red clump may provide important constraints to the star formation history of nearby galaxies, as well as to the distribution of their stars along the line-of-sight.

Acknowledgments

Thanks are due to E. Bica, A. Bressan, C. Chiosi and A. Weiss for their useful comments and suggestions. A.A. Cole and L. Gardiner are acknowledged for calling our attention to some important observational work here mentioned (regarding NGC 752 and the SMC, respectively). A.A. Cole, J.S. Gallagher and J.A. Holtzman kindly provided the data for Fig. 10. We made use of the Simbad database, mantained by the CDS, Strasbourg. This work is funded by the Alexander von Humboldt-Stiftung.

References

Alongi M., Bertelli G., Bressan A., Chiosi C., Fagotto F., Greggio L., Nasi E., 1993, A&AS 97, 851

Alves D.R., Basu A., Cook K.H., et al., 1998, in New Views of the Magellanic Clouds, IAU Symp. 190, eds. Chu Y.-H., Suntzeff N., Hesser J., Bohlender D., in press (astro-ph/9810221).

Beaulieu J.-P., Sackett P.D., 1998, AJ 116, 209

Becker S.A., Iben I. Jr., 1980, ApJ 237, 111
Bertelli G., Mateo M., Chiosi C., Bressan A., 1992, ApJ 388, 400
Bertelli G., Bressan A., Chiosi C., Fagotto F, Nasi E., 1994, A&AS, 106, 275
Bica E., Clariá J.J., Dottori H., Santos Jr. J.F.C., Piatti A.E., 1996, ApJS 102, 57
Bica E., Geisler D., Dottori H., Clariá J.J., Piatti A.E., Santos Jr. J.F.C., 1998, AJ 116, 723
Cannon R.D., 1970, MNRAS 150, 111
Carraro G., Chiosi C., 1994, A&A 287, 761
Castellani V., Chieffi A., Straniero O., 1992, ApJS 78, 517
Chiosi C., Bertelli G., Bressan A., 1992, ARA&A 30, 235
Cole A.A., 1998, ApJ 500, L137
Corsi C.E., Buonanno R., Fusi Pecci F., Ferraro F.R., Testa V., Greggio L., 1994, MNRAS 271, 385
Da Costa G., 1991, in The Magellanic Clouds, IAU Symp. 148, eds. Haynes R., Milne D., Dordrecht: Kluwer, p. 183
Da Costa G., Hatzidimitriou D., 1998, AJ 115, 1934
Daniel S.A., Latham D.W., Mathieu R.D., Twarog B.A., 1994, PASP 106, 281
Elson R.A.W., Fall S.M., 1985, ApJ 299, 211
ESA, 1997, The Hipparcos and Tycho Catalogues, ESA SP-1200
Faulkner D.J., Cannon R.D., 1973, ApJ 180, 435
Gardiner L.T., Hawkins M.R.S., 1991, MNRAS 251, 174
Gardiner L.T., Hatzidimitriou D., 1992, MNRAS 257, 195
Geisler D., Bica E., Dottori H., Clariá J.J., Piatti A.E., Santos Jr. J.F.C., 1997, AJ 114, 1920
Geha M.C., Holtzman J.A., Mould J.R., et al., 1998, 115, 1045
Girardi L., Chiosi C., Bertelli G., Bressan A., 1995, A&A 298, 87
Girardi L., 1998, in New Views of the Magellanic Clouds, IAU Symp. 190, eds. Chu Y.-H., Suntzeff N., Hesser J., Bohlender D., in press.
Girardi L., Bertelli G., 1998, MNRAS 300, 533
Girardi L., Groenewegen M.A.T., Weiss A., Salaris M., 1998, MNRAS 301, 149
Girardi L., Bressan A., Bertelli G., Chiosi C., 1999, in preparation
Gratton R., Fusi Pecci F., Carretta E., Clementini G., Corsi C.E., Lattanzi M., 1997, ApJ 491, 749
Gratton R., Carretta E., Clementini G., 1998, in Post-Hipparcos Standard Candles, eds. A. Heck & F. Caputo, Kluwer: Dordrecht, in press.
Hatzidimitriou D., 1991, MNRAS 251, 545
Hatzidimitriou D., Hawkins M.R.S., 1989, MNRAS 241, 667
Hatzidimitriou D., Cannon R.D., Hawkins M.R.S., 1993, MNRAS 261, 873
Heintz W.D., 1982, PASP 94, 705
Holtzman J.A., Mould J.R., Gallagher J.S., et al., 1997, AJ 113, 656
Ibata R.A., Lewis G.F., Beaulieu J.-P., 1998, ApJ 509, L29
Kurucz R.L., 1992, in The Stellar Populations of Galaxies, eds. B. Barbuy and A. Renzini, Dordrecht: Kluwer, p. 225
Maeder A., Meynet G., 1989, A&A 1989 210, 155
Mateo M., Hodge P., Schommer R.A., 1986, ApJ 311, 113
McWilliam A., 1990, ApJS 74, 1075
Mermilliod J.-C., Mathieu R.D., Latham D.W., Mayor M., 1998, A&A 339, 423
Olszewski E.W, Schommer R.A., Suntzeff N.B., Harris H.C., 1991, AJ 101, 515
Olszewski E.W, Suntzeff N.B., Mateo M., 1996, ARA&A 34, 511
Paczyński B., Stanek K.Z., 1998, ApJ 494, L219
Perryman M.A.C., et al., 1997, A&A 323, L49
Popowski P., Gould A., 1998, in Post-Hipparcos Standard Candles, eds. A. Heck & F. Caputo, Kluwer: Dordrecht, in press.
Reimers D., 1975, Mem. Soc. R. Sci. Liège, ser. 6, vol. 8, p. 369
Renzini A., Fusi Pecci F., 1988, ARA&A 26, 199
Salaris M., Weiss A., 1997, A&A 327, 107
Salaris M., Weiss A., 1998, A&A 335, 943
Sarajedini A., 1998, AJ 116, 738
Searle L., Sargent W.L.W., 1972, ApJ 173, 25
Seidel E., Demarque P., Weinberg D., 1987, ApJS 63, 917
Seidel E., Da Costa G.S., Demarque P., 1987, ApJ 313, 192
Smecker-Hane T., Gallagher J.S., Cole A.A., Tolstoy E., Stetson P.B., 1998, in New Views of the Magellanic Clouds, IAU Symp. 190, eds. Chu Y.-H., Suntzeff N., Hesser J., Bohlender D., in press.
Stanek K.Z., Garnavich P.M., 1998, ApJ 503, L131
Stanek K.Z., Zaritsky D., Harris J., 1998, ApJ 500, L141
Stappers B.W., Mould J.R., Sebo K.M., et al., 1997, PASP 109, 292
Sweigart A.V., Greggio L., Renzini A., 1989, ApJS 69, 911
Sweigart A.V., Greggio L., Renzini A., 1990, ApJ 364, 527

Tolstoy E., Gallagher J.S., Cole A.A., Hoessel J.G., Saha A., Dohm-Palmer R., Skillman E., Mateo M., Hurley-Keller D., 1998, AJ 116, 1244
Udalski A., Szymański M., Kubiak M., Pietrzyński G., Woźniak P., Żebruń K, 1998, Acta Astr. 48, 1
Udalski A., 1998a, Acta Astr. 48, 113
Udalski A., 1998b, Acta Astr. 48, 383
Vallenari A., Chiosi C., Bertelli G., Aparicio A., Ortolani S., 1996 A&A 309, 367
Zaritsky D., Lin D.N.C, 1997, AJ 114, 2545
Zinn R., West M.J., 1984, ApJS 55, 45

This article was processed by the author using a modified version of the Springer-Verlag LaTeX A&A style file *L-AA* version 3.